Role of Pore Structure of Activated Carbon Fibers in the Catalytic Oxidation of H 2 S

ARTICLE *in* INDUSTRIAL & ENGINEERING CHEMISTRY RESEARCH · APRIL 2010

Impact Factor: 2.59 · DOI: 10.1021/ie901223j

Role of Pore Structure of Activated Carbon Fibers in the Catalytic Oxidation of H_2S

Qingjun Chen, Zhi Wang, Donghui Long, Xiaojun Liu, Liang Zhan, Xiaoyi Liang, Wenming Qiao, and Licheng Ling*

State Key Laboratory of Chemical Engineering, East China University of Science and Technology, Shanghai 200237, China

Na_2CO_3-impregnated activated carbon fibers (ACFs) have been developed as low-concentration H_2S oxidation catalysts at ambient temperature. Two series of commercial pitch-based and poly(acrylonitrile)-based ACFs were used to evaluate the role of pore structure in the oxidation of H_2S. The initial, impregnated, and exhausted materials were characterized using elemental analysis, N_2 adsorption, scanning electron microscopy (SEM), thermogravimetry analysis, and activity tests. The catalytic oxidation of H_2S continued until all effective pores of the catalysts were blocked by the oxidation products. The saturation sulfur capacity was found to be in the range of 0.10−0.81 g of H_2S/g of catalyst, with the value strongly dependent on the pore structure (especially the volume of pores larger than 0.7 nm) but independent of the nitrogen functional groups. Further quantitative analysis suggested that elemental sulfur as a dominant product mostly deposited in large pores (d > 0.7 nm), whereas sulfuric acid was preferably produced in small micropores (d < 0.7 nm). A possible mechanism of H_2S oxidation with respect to the pore size of catalysts is proposed.

1. Introduction

Hydrogen sulfide (H_2S) is one of the leading malodorants arising from natural gas,[1] digester gas,[2] geothermal wells,[3] and municipal sewage treatment facilities.[4−6] Many processes have been developed to deal with H_2S removal, including wet scrubbing,[7,8] the Claus process,[9,10] biological methods,[11] and catalytic-oxidation processes.[12,13] Among these, the method of catalytic oxidation of H_2S to elemental sulfur, which does not require preliminary treatment of the gases or concentration of the hydrogen sulfide, is most promising.[12,13]

Porous carbon materials have been widely used for H_2S catalytic oxidation because of their unique pore structure and modifiable surface chemistry.[14,15] Although it has been reported that the sulfur capacity of unmodified activated carbons is significant for low-concentration H_2S removal at a low space velocity of the gas stream,[16] alkali-impregnated porous carbons are still the first choice for H_2S removal because of their large sulfur capacities and fast kinetics of reaction.[17,18]

For impregnated carbons, understanding the effect of pore structure on the performance of these materials for H_2S removal is a scientifically and technologically important problem, which could enable the design of more efficient H_2S oxidation catalysts. Much attention has been paid to investigating the influence of operating conditions such as oxygen concentration,[12] relative humidity,[19] and space velocity,[20] as well as the role of impregnated alkalis in the oxidation of H_2S.[21−23] However, the effect of pore structure (specific surface area, pore volume, and pore size distribution) on the performance of impregnated carbons for H_2S oxidation is still an open question. Bandosz et al. suggested that the performance of impregnated carbons was dominated only by the amount of active base and that the capacity per unit volume of carbon bed was insensitive to the surface area and pore structure.[21] On the other hand, as reported by Yan et al.,[17,22] Ros et al.,[23] and Xiao et al.,[12] both physical porosity and surface chemistry (such as pH value) have been found to be important factors influencing the performance of alkali-impregnated activated carbons for H_2S removal.

The mechanism of H_2S oxidation over activated carbons is also widely debated. Steijns et al. concluded that the as-produced sulfur catalyzed H_2S oxidation and that the activity was a function of the amount of adsorbed sulfur.[24] Bagreev et al. considered that the oxidation took place at three different active sites, namely, sulfur, surface carbons, and impregnated NaOH, and proposed three oxidation pathways for these three types of active sites.[21] Yan et al. investigated the effect of pH on H_2S oxidation and proposed a mechanism depending on the pH value.[17] Thus, the mechanism of H_2S oxidation needs to be further studied.

The objective of this work was to elucidate the correlation between pore structure and H_2S removal performance of Na_2CO_3-impregnated activated carbon fibers (ACFs) and to study the reaction mechanism. The results indicated that the pore structure of the catalysts plays an important role in the catalytic oxidation of H_2S. The saturation sulfur capacity was dominated by the volume of pores larger than 0.7 nm, and two possible pathways for H_2S oxidation in pores with different sizes were identified.

2. Experimental Section

2.1. Preparation of the Catalysts. The two series of activated carbon fibers used in this work are denoted as pitch-based ACFs (P1, P2, and P3) and poly(acrylonitrile)- (PAN-) based ACFs (N1, N2, and N3) and were obtained from Osaka Gas Co. Ltd. (Osaka, Japan) and Toho Tenax Co. Ltd. (Tokyo, Japan), respectively. Activation was performed by the steam activation method, and the degree of activation increased with increasing assigned number (i.e., P3 and N3 were most highly activated). The main variable factor was the activation time (the exact activation times and temperatures were not provided by the suppliers). The elemental compositions of the ACFs are collected in Table 1.

The catalysts were prepared by wetness impregnation, which has been described elsewhere.[25] In detail, 0.6 g of ACF was immersed in 10 mL of 6 wt % Na_2CO_3 solution for 24 h, and the solution was then filtered. The obtained sample was dried at 120 °C for 24 h to remove the adsorbed water before use. The impregnated samples are designated with a letter I added

* To whom correspondence should be addressed. Tel.: (86) 21 64252934. Fax: (86) 21 64252914. E-mail: lchling@ecust.edu.cn.

10.1021/ie901223j
Published on Web 02/25/2010

Table 1. Elemental Compositions of the Samples

sample	C (wt %)	H (wt %)	N (wt %)	O[a] (wt %)
P1	92.40	0.81	0.83	5.86
P2	93.31	0.85	0.57	5.27
P3	93.66	0.87	0.49	4.98
N1	80.92	1.21	10.02	7.85
N2	82.31	1.20	4.56	11.93
N3	83.60	1.38	2.48	12.54

[a] Oxygen content was calculated by difference.

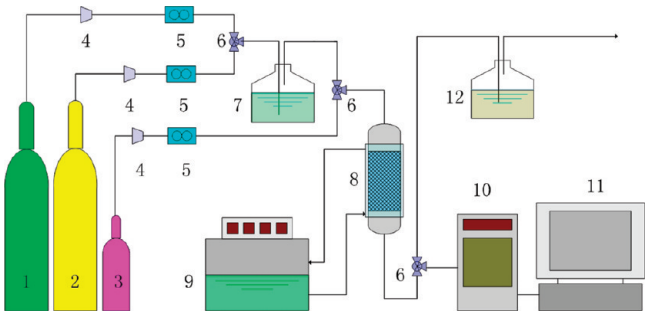

Figure 1. Schematic diagram of the experimental system: (1) cylinder of N_2, (2) cylinder of O_2 and N_2, (3) cylinder of H_2S and N_2, (4) pressure regulator, (5) mass flow controller, (6) triple valve, (7) humidifier, (8) reactor, (9) cyclic water bath, (10) H_2S analyzer, (11) computer, (12) NaOH solution.

to the sample name, and the exhausted activated carbon fibers are designated by the additional letter E.

2.2. Activity Tests of Impregnated ACFs for H_2S Removal. The experimental setup is shown in Figure 1. Catalysts were packed in a glass tube with a diameter of 4 mm and a height of 20 mm. A simulated mixture (99% of N_2 and 1% of O_2 at 30 °C) containing 0.1% (1000 ppm) H_2S (with 80% relative moisture) was passed through the column of the catalysts at a flow rate of 150 mL/min. The gas flow rates were controlled with a mass flow controller system (ZF-MFC-1, Shanghai Zufa Co.). The H_2S emission was monitored by a Shuangyang LC-2 H_2S continuous monitor system (electrochemical detector) interfaced with a computer data acquisition program. The test was stopped at the point that the elution concentration was approximately equal to the inlet concentration and did not change with time. For each sample, the test was repeated at least twice.

The adsorption/removal capacity, Q (in grams of H_2S per gram of catalyst), was calculated by integrating the corresponding breakthrough curve using the equation

$$Q = \frac{qM_W}{1000wV_M}\left[C_0 t_s - \int_0^{t_s} C(t)\,dt\right] \quad (1)$$

where q is the total inlet flow rate (m^3/s), w is the weight of catalyst introduced into the column (g), M_W is the molecular weight of H_2S, V_M is the molar volume, C_0 is the inlet gas H_2S concentration (ppmv), $C(t)$ is the outlet gas concentration (ppmv), and t_s is the H_2S breakthrough/saturation time(s). In this test, the breakthrough concentration of H_2S is defined as 50 ppmv. The breakthrough and saturation sulfur capacities are denoted as Q_B and Q_S, respectively.

2.3. Characterization. Elemental analysis of the ACFs was carried out using a Vario EL III element analyzer (Sartorius GmbH). The samples were dried at 120 °C for 3 h before measurement. N_2 adsorption−desorption isotherms of the samples were measured using a Micromeritics ASAP 2020 M analyzer at −196 °C. The specific surface area (S_{BET}) was calculated by the Brunauer−Emmett−Teller (BET) method. The total pore volume (V_t), the volumes of pores smaller and larger than 0.7 nm ($V_{<0.7}$ and $V_{>0.7}$, respectively), and the pore size distributions were calculated using nonlocal density functional theory (DFT). The morphology of the samples was observed by scanning electron microscopy (SEM, FEI Q-300). Thermogravimetry analysis (TA Instrument Q600 Analyzer) of the samples was carried out in nitrogen at a flow rate of 100 mL/min. The samples were heated to 1000 °C at a rate of 10 °C/min. The pH values of the samples were measured by a PHS-3B pH analyzer. The samples (0.1 g) were placed in 20 mL of water and equilibrated overnight. Then, the flask contents were filtered, and the pH values were measured.

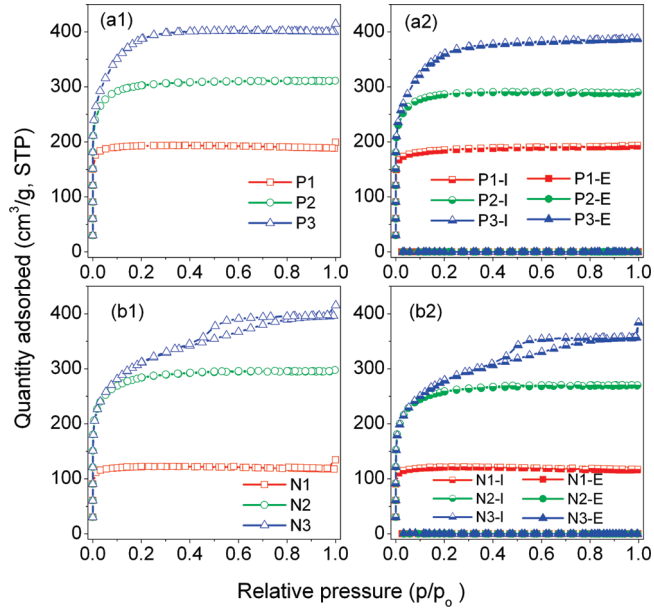

Figure 2. N_2 adsorption−desorption isotherms of the (a1,a2) pitch-based and (b1,b2) PAN-based ACFs.

3. Results

3.1. Pore-Structure Analysis of Original, Impregnated, and Exhausted ACFs. N_2 adsorption−desorption isotherms of the original ACFs are shown in Figure 2. The pore-structure parameters are summarized in Table 2. All original ACFs, except N3, exhibited type I isotherms according to the classification of IUPAC,[26] indicating that the ACFs are mainly microporous materials. In the case of N3, a hysteresis loop was observed at a high relative pressure, demonstrating the presence of some mesopores. For the pitch-based ACFs, the specific surface area and total pore volume both increased in the order P1 < P2 < P3. For the PAN-based ACFs, they both increased in the order N1 < N2 < N3, corresponding to their activation degrees. Among the two series of original ACFs, P3 showed the highest specific surface area (1275 m^2/g) and largest total pore volume (0.55 cm^3/g), whereas N1 exhibited the smallest specific surface area (366 m^2/g) and total pore volume (0.17 cm^3/g). The pore size distributions of the original ACFs are presented in Figure 3. The pore size distributions became broader from P1 to P3 and from N1 to N3.

The impregnation of Na_2CO_3 resulted in some changes in the pore structure of the ACFs. The nitrogen adsorption−desorption isotherms of the impregnated ACFs are also presented in Figure 2. The N_2 adsorption capacity decreased after impregnation, and both the specific surface area and total pore volume also decreased. For most of the ACFs, the content of

Table 2. Pore-Structure Parameters and pH Values of the Samples

sample	S_{BET} (m^2/g)	V_t (cm^3/g)	$V_{<0.7}$[a] (cm^3/g)	$V_{>0.7}$[b] (cm^3/g)	$V_{<0.7}/V_t$	$V_{>0.7}/V_t$	D_m (nm)	pH
P1	600	0.24	0.15	0.09	0.63	0.37	1.95	6.23
P2	1002	0.40	0.14	0.26	0.35	0.65	2.00	5.93
P3	1275	0.55	0.11	0.44	0.20	0.80	1.94	5.73
N1	366	0.17	0.11	0.06	0.64	0.35	1.99	6.24
N2	878	0.38	0.13	0.25	0.34	0.66	2.08	6.09
N3	1008	0.54	0.12	0.42	0.22	0.78	2.43	5.61
P1-I	561	0.24	0.16	0.08	0.67	0.33	2.12	9.66
P2-I	910	0.38	0.14	0.24	0.37	0.63	2.04	10.03
P3-I	1147	0.52	0.12	0.41	0.23	0.77	2.09	9.76
N1-I	362	0.15	0.10	0.05	0.67	0.33	1.98	9.31
N2-I	763	0.35	0.11	0.24	0.31	0.69	2.08	9.92
N3-I	886	0.51	0.12	0.39	0.24	0.76	2.44	9.83
P1-E	0	0.02	0.01	0.01	0.50	0.50	nd[c]	2.54
P2-E	nd	nd	nd	nd	nd	nd	nd	3.78
P3-E	nd	nd	nd	nd	nd	nd	1.25	7.86
N1-E	0.31	0.00	0.00	0.00	nd	nd	nd	2.89
N2-E	nd	nd	nd	nd	nd	nd	nd	3.65
N3-E	0.45	0.00	0.00	0.00	nd	nd	nd	6.50

[a] Volume of pores with sizes smaller than 0.7 nm. [b] Volume of pores with sizes greater than 0.7 nm. [c] nd, could not be calculated from the isotherms using the BET or DFT methods.

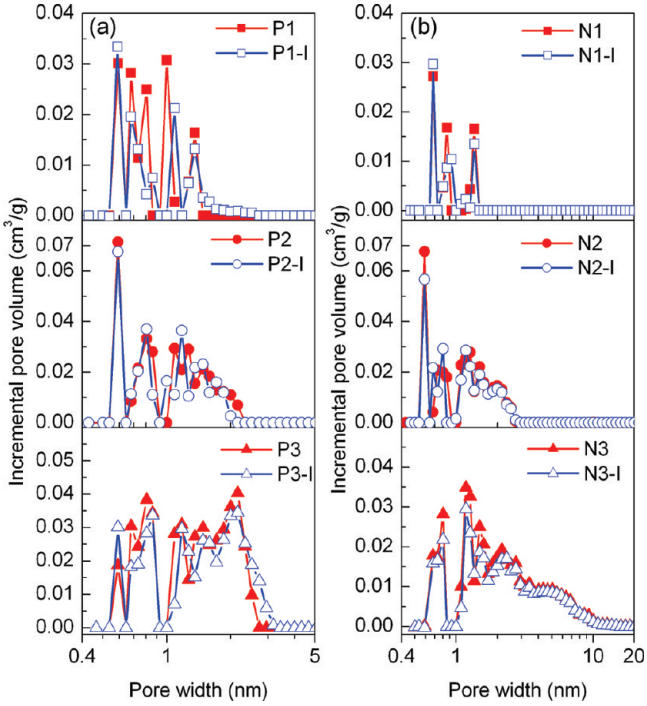

Figure 3. Pore size distributions of the (a) pitch-based and (b) PAN-based ACFs before and after impregnation.

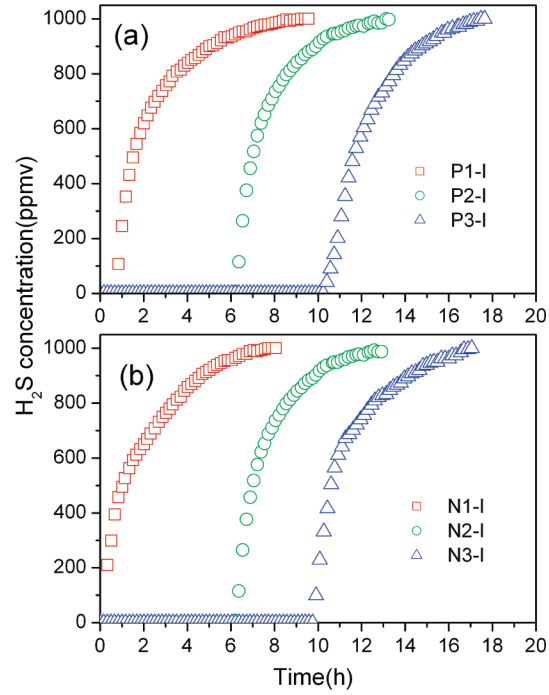

Figure 4. Breakthrough curves of H_2S over the (a) pitch-based and (b) PAN-based catalysts.

large pores ($V_{>0.7}/V_t$) decreased, whereas the content of small micropores ($V_{<0.7}/V_t$) increased slightly (Table 2) after impregnation. This result indicates that Na_2CO_3 mainly deposited in the large pores ($d > 0.7$ nm).

The DFT pore size distributions of original and impregnated samples are shown in Figure 3. After impregnation, the volume of large pores ($d > 0.7$ nm) decreased obviously, whereas that of small micropores ($d < 0.7$ nm) increased or only slightly decreased. This result further confirms that most of the Na_2CO_3 deposited in the large pores ($d > 0.7$ nm). However, impregnation did not change the pore size distributions significantly, as shown in Figure 3. The impregnated ACFs exhibited pore structures similar to those of the original ACFs.

After desulfurization, the N_2 adsorption capacity could not be detected for all samples, as can be seen from Figure 2. This result suggests that almost all of the pores of the exhausted ACFs were filled or blocked by the products of H_2S oxidation.

3.2. Performance of Impregnated ACFs for H_2S Removal. Breakthrough curves of H_2S over the two series of impregnated ACFs are shown in Figure 4. H_2S adsorption/removal capacities calculated from breakthrough curves are reported in Table 3. The shapes of the breakthrough curves of the two series of impregnated ACFs are similar, but the breakthrough and saturation times are different. The largest saturation sulfur capacity of 0.81 g of H_2S/g of catalyst was obtained for P3-I, whereas the smallest saturation sulfur capacity

Table 3. H_2S Adsorption/Removal Capacities of the Samples

sample	Q_B (g/g)	Q_S (g/g)
P1-I	0.05	0.17
P2-I	0.42	0.50
P3-I	0.71	0.81
N1-I	0.03	0.10
N2-I	0.44	0.52
N3-I	0.69	0.78

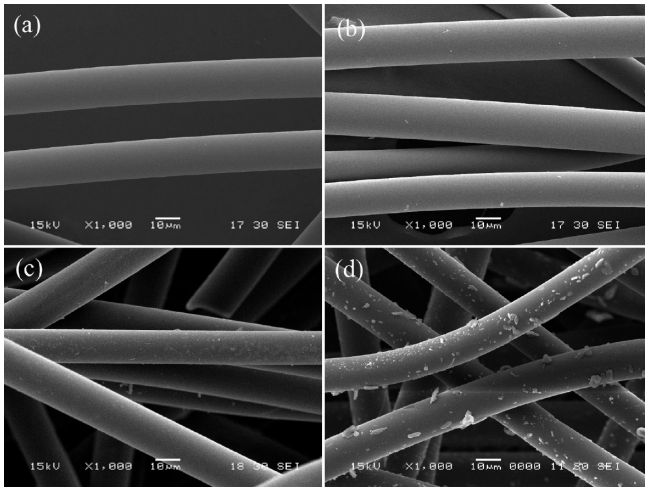

Figure 5. SEM images of the (a) original (P3), (b) impregnated (P3-I), and (c) exhausted (P3-E) ACFs and of the (d) exhausted ACFs after having been dried at 120 °C for 24 h (P3-E).

of 0.10 g of H_2S/g of catalyst was achieved for N1-I. The saturation sulfur capacities of the pitch-based and PAN-based catalysts increased in the orders P1-I < P2-I < P3-I and N1-I < N2-I < N3-I, respectively.

3.3. Products of H_2S Oxidation over Impregnated ACFs. SEM images of original, impregnated, and exhausted ACFs are presented in Figure 5. The original ACFs (Figure 5a) had smooth surfaces. After impregnation, no significant changes were found, except for the presence of some small solid Na_2CO_3 particles (Figure 5b). The surfaces of the exhausted ACFs were still smooth, but some small floc-like solids appeared. After the samples had been dried at 120 °C for 24 h, many particles with the size of several micrometers were present on the surfaces of the exhausted ACFs, which should be the oxidation product elemental sulfur.[23,27−29] It was found that the pH values of the catalysts decreased significantly after H_2S oxidation (shown in Table 2). This result indicates that some acid materials were also produced during the oxidation process.

Table 4. Different Species Desorbed Calculated from the TG−DTG Curves

	weight loss (%)				sulfur species (wt %)	
sample	water (0−150 °C)	sulfur oxides	elemental sulfur	other gases (500−1000 °C)	SO_x	S
P1-E	3.17	5.38[a]	7.65[a]	7.84	38.99	61.01
P2-E	3.30	5.81[b]	26.25[b]	8.48	18.12	81.88
P3-E	4.15	6.43[c]	36.85[c]	9.68	14.86	85.14
N1-E	4.06	3.98[d]	9.17[d]	11.58	30.27	69.73
N2-E	4.41	7.45[c]	24.75[c]	15.27	20.83	79.17
N3-E	4.41	6.67[e]	37.79[e]	14.13	15.45	84.55

[a] Sulfur oxides, 150−300 °C; elemental sulfur, 300−500 °C. [b] Sulfur oxides, 150−280 °C; elemental sulfur, 280−500 °C. [c] Sulfur oxides, 150−270 °C; elemental sulfur, 270−500 °C. [d] Sulfur oxides, 150−250 °C; elemental sulfur, 250−500 °C. [e] Sulfur oxides, 150−230 °C; elemental sulfur, 230−500 °C.

Thermogravimetry analysis can provide some quantitative and qualitative information about the products of H_2S oxidation. Figure 6 presents the TG−DTG curves of the exhausted ACFs. According to the literature,[21,22,30−33] the weight loss in the range of 150−500 °C is due to the desorption of sulfur species from exhausted ACFs. In the DTG curves, two peaks (or shoulders) can be observed in the 150−500 °C range, where the first peak (or shoulder, at a lower temperature) is assigned to the desorption of SO_x and the second peak (at a higher temperature) is assigned to the desorption of elemental sulfur.[21,22,30−33] A detailed analysis of the sulfur species desorbed from TG−DTG curves is presented in Table 4. It is obvious that the weight loss of elemental sulfur is significantly greater than that of SO_x for all exhausted ACFs. Thus, the main product of H_2S oxidation over impregnated ACFs is elemental sulfur. The content of elemental sulfur in the oxidation products was about 61−85%. It was also found that the content of elemental sulfur increased

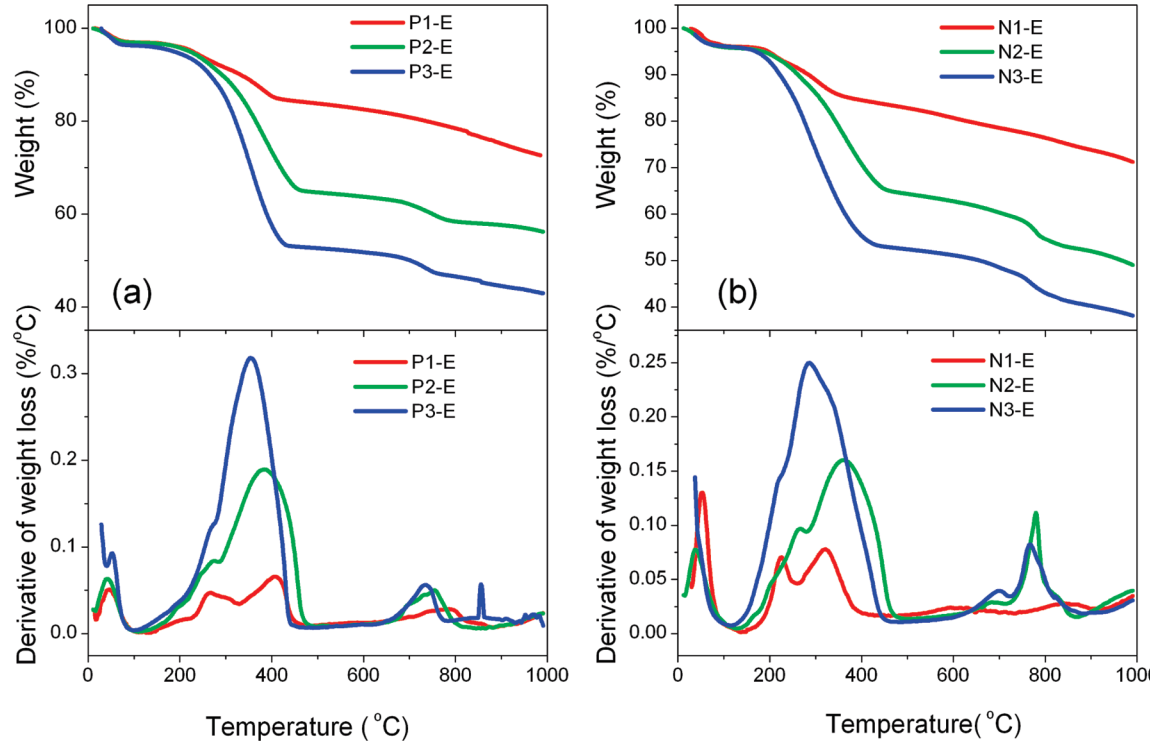

Figure 6. TG−DTG curves of the (a) pitch-based and (b) PAN-based exhausted ACFs.

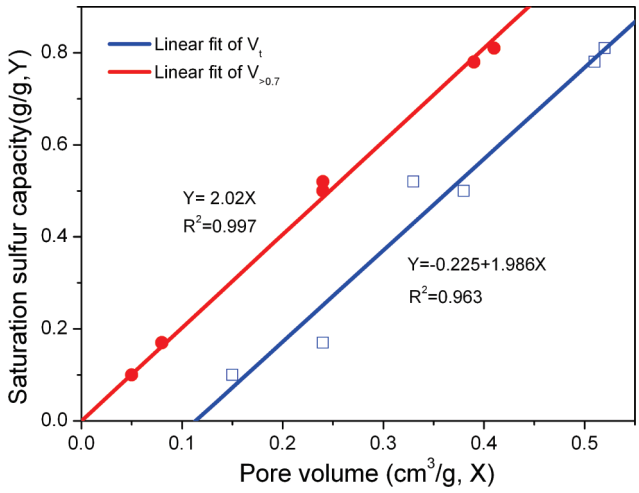

Figure 7. Relationships between saturation sulfur capacity and pore volume.

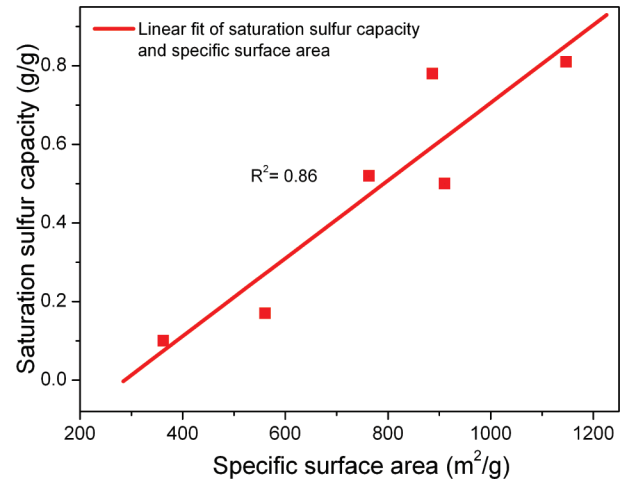

Figure 8. Correlation between saturation sulfur capacity and specific surface area.

with increasing pore volume of the catalysts, whereas the content of sulfur oxides had the reverse tendency.

4. Discussion

4.1. Effect of Pore Structure on Performance of Impregnated ACFs. Pore structure has a significant effect on the performance of impregnated ACFs for H_2S removal. A regression analysis was performed to correlate the saturation sulfur capacity and pore volume, as presented in Figure 7. A linear relationship ($R^2 = 0.963$) between total pore volume and saturation sulfur capacity was obtained, which suggests that the saturation sulfur capacity strongly depends on the total pore volume. Assuming that all of the pores were completely filled by the dominant oxidation product, elemental sulfur, the saturation sulfur capacity for P3-I would be ca. 1.02 g of H_2S/g of catalyst (supposing the density of elemental sulfur to be 1.96 g/cm^3). However, the saturation sulfur capacity calculated from the breakthrough curve is only 0.81 g of H_2S/g of catalyst, which means that some of the pores were not completely filled with elemental sulfur.

It should be pointed out that the saturation sulfur capacity exhibited a very good linear relationship with the volume of large pores ($d > 0.7$ nm) (Figure 7), described by the equation $Q_S = 2.02$ g/$cm^3 \times V_{>0.7}$ ($R^2 = 0.997$), where Q_S is the saturation sulfur capacity, $V_{>0.7}$ is the volume of large pore ($d > 0.7$ nm), and R^2 is the correlation coefficient. The straight line through the origin represents direct proportionality between the saturation sulfur capacity and the volume of large pores. Furthermore, the proportionality coefficient of 2.02 g/cm^3 approximately equals the density of elemental sulfur (1.96−2.07 g/cm^3). That is, the large pores ($d > 0.7$ nm) were completely filled with elemental sulfur.

The correlation between the saturation sulfur capacity and the specific surface area is displayed in Figure 8. A linear relationship is observed. However, samples exhibiting larger surface areas did not always give larger saturation sulfur capacities. For example, the specific surface area of P2-I was larger than those of N2-I and N3-I, but its saturation sulfur capacity was smaller than theirs. Furthermore, all porosities of the impregnated ACFs vanished after desulfurization, as indicated by the N_2 adsorption results, which reveals that the products of the oxidation were closely packed in the pores instead of covering on the surface. Therefore, it can be concluded that pore volume rather than specific surface area played a dominant role in the saturation sulfur capacities of the catalysts.

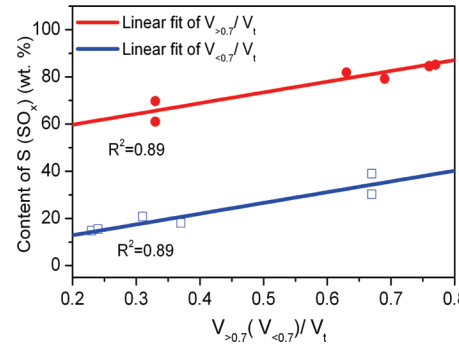

Figure 9. Relationships between the content of S (SO_x) and the ratios $V_{>0.7}/V_t$ and $V_{<0.7}/V_t$.

4.2. Effect of Nitrogen-Containing Groups on Performance of Impregnated ACFs. It is hoped that the nitrogen atoms contained in the PAN-based ACFs could play a positive role in H_2S removal.[13,34] However, samples P2-I and N2-I, which had similar pore structures but different amounts of nitrogen, exhibited similar saturation sulfur capacities. It can therefore be concluded that nitrogen-containing groups do not make any difference in the performances of impregnated ACFs with similar pore structures. Furthermore, the saturation sulfur capacities of the impregnated ACFs were found to be directly proportional to the volume of large pores irrespective of the nitrogen content. These results reveal that nitrogen functional groups have a negligible effect on H_2S removal over impregnated ACFs. A possible explanation for this finding is that impregnated ACFs exhibit very high activities and can endlessly oxidize H_2S to elemental sulfur (or SO_x) until all space is blocked, whereas the possible effects of nitrogen surface groups cannot be displayed. More definitive information should be required to explain the effects of surface chemistry.

4.3. Effect of Pore Structure on Products of H_2S Oxidation over Impregnated ACFs. Pore structure also affects the products of H_2S oxidation over impregnated ACFs. As seen from Tables 2 and 4, the distributions of products were different for impregnated ACFs with different pore structures. The impregnated ACF exhibiting more pores larger than 0.7 nm produced more elemental sulfur, whereas that showing more small micropores produced more sulfur oxides. The correlation between the content of elemental sulfur and the ratio of large pores ($V_{>0.7}/V_t$) is shown in Figure 9. A linear relationship can be observed, which indicates that H_2S is mainly oxidized to

elemental sulfur in the large pores ($d > 0.7$ nm). On the other hand, the linear relationship between the content of SO_x and the ratio of small micropores ($V_{<0.7}/V_t$) indicates that H_2S is mainly oxidized to SO_x in the small micropores (Figure 9). These results suggest that elemental sulfur is preferably formed in large pores whereas H_2SO_4 is mainly produced in small micropores.

4.4. Effect of Pore Structure on Mechanism of H_2S Oxidation. From various pieces of evidence gathered from the literature,[12,13,17,21−23,27,31,34−38] the oxidation of H_2S over impregnated ACFs can be divided into the following four steps: (1) Infinitely thin water films are formed in the micropores and even mesopores of impregnated ACFs, resulting from water accumulation and condensation in the presence of moisture. (2) H_2S dissolves in the water films and dissociates into HS^- ions. (3) O_2 dissociates into dissociatively adsorbed oxygen (O*).[14,19,27,31,36] (4) HS^- reacts with O* to form elemental sulfur or sulfur oxides. Four types of groups could be the active sites for the catalytic oxidation of H_2S: nitrogen-containing groups,[13,34,39] impregnation agents,[21] edge (or defect) carbon atoms,[21,40] and elemental sulfur (or polysulfides).[21,24,41] Nitrogen-containing groups might play an important role in the oxidation of H_2S on original activated carbons, but according to the results obtained in this study, they do not have significant effects on impregnated ACFs. The role of alkali impregnants is widely accepted as promoting the dissolution and dissociation of H_2S in water films through acid−base reactions rather than active sites for the oxidation of H_2S.[12,15,17,22]

In our opinion, the active sites of the oxidation reaction should be edge (or defect) carbon atoms, where the density of the electron cloud is intensified and O_2 can be easily captured. The captured O_2 can dissociate into dissociatively adsorbed oxygen (O*). At the active sites, the process includes the following steps

$$C_f + O_2 \rightarrow C{-}O_2(ads) \quad (2)$$

$$C{-}O_2(ads) \rightarrow 2C{-}O^* \quad (3)$$

where C_f, $C{-}O_2$(ads), and C−O* represent carbon active sites, chemisorbed oxygen, and dissociatively adsorbed oxygen at carbon sites, respectively.

The dissociatively adsorbed oxygen can oxidize HS^- to elemental sulfur or sulfur oxides depending on the reaction energy provided by the catalysts. In the presence of water and oxygen, the oxidation of H_2S over Na_2CO_3-impregnated ACFs can be represented by the equations

$$H_2S + H_2O \rightarrow HS^- + H_3O^+ \quad (4)$$

$$H_2S + CO_3^{2-} \rightarrow HS^- + HCO_3^- \quad (5)$$

$$H_2S + HCO_3^- \rightarrow HS^- + H_2CO_3 \quad (6)$$

$$C{-}O^* + HS^- \rightarrow C_f + S^* + OH^- \quad (7)$$

$$xS^* \rightarrow S_x \quad (8)$$

$$S^* + O_2 \rightarrow SO_2 \quad (9)$$

$$SO_2 + 0.5O_2 + H_2O \rightarrow SO_4^{2-} + 2H^+ \quad (10)$$

where S* and S_x represent sulfur radicals (or small sulfur chains) and sulfur polymers (or elemental sulfur), respectively.

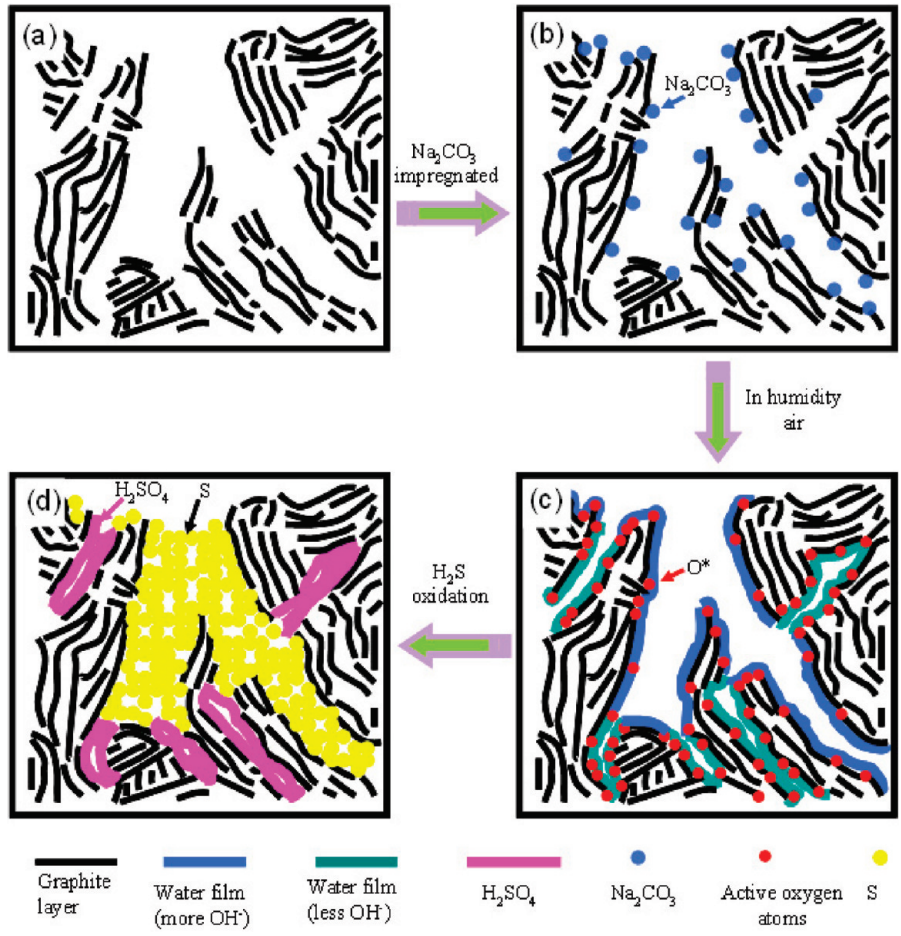

Figure 10. Schematic representation of H_2S oxidation and sulfur species deposition in the pores: (a) original ACFs; (b) impregnated ACFs; and (c,d) ACFs before and after desulfurization, respectively.

Small micropores ($d < 0.7$ nm) are favored for forming high concentrations of dissociatively adsorbed oxygen because of their high surface energy. Therefore, it is feasible for HS^- to be oxidized to sulfur radicals or small sulfur chains and then further oxidized to H_2SO_4 in small micropores.[22,31,32] In large pores ($d > 0.7$ nm), more carbonate sodium is deposited, as revealed by N_2 adsorption, so the concentration of HS^- in the water films is relative high. In addition, the density of active sites and the concentration of dissociatively adsorbed oxygen in large pores are lower than those in small micropores. Also, the elemental sulfur, generally in the form of S_8 clusters, could not be stored in the small micropores because of space limitation. As a result, the intermediate oxidation product, elemental sulfur, rather than H_2SO_4 is formed in the large pores. The as-formed elemental sulfur can be transferred from the active sites by the water films. The continuous cleaning of the active sites by water allows for the maintenance of the activity of the active sites.[12,28] Meanwhile, the accumulation of sulfur can form large sulfur particles, which deposits in the pores of the catalyst. The elemental sulfur (or polysulfides) might also be the active sites for H_2S oxidation.[21,24,41] In addition to eqs 2−10, in large pores, the oxidation mechanism will also involve the following steps

$$S_x + HS^- \rightarrow HS_xS^- \quad (11)$$

$$HS_xS^- + 0.5O_2 \rightarrow HS_xS^-O^* \quad (12)$$

$$HS_xS^-O^* + HS^- \rightarrow HS_{x+1}S^- + OH^- \quad (13)$$

$$HS_xS^-O^* + 0.5O_2 \rightarrow HS_{x-1}S^- + OH^- + SO_2 \quad (14)$$

$$SO_2 + 0.5O_2 + OH^- \rightarrow SO_4^{2-} + H^+ \quad (15)$$

$$2H_2S + SO_2 \rightarrow 3S + 2H_2O \quad (16)$$

where HS_xS^- ($HS_{x-1}S^-$, $HS_{x-1}S^-$) and $HS_xS^-O^*$ represent polysulfides ions and dissociatively adsorbed oxygen at sulfur sites, respectively.

The impregnated ACFs will not be deactivated until the large pores are completely filled by elemental sulfur. Because elemental sulfur is the dominant product and mostly deposits in the large pores, the saturation sulfur capacity of the impregnated ACFs is mainly determined by the volume of the large pores.

Based on the Norit model for pores of activated carbons,[42] a schematic representation of H_2S oxidation occurring in the pores of impregnated ACFs is presented in Figure 10. Na_2CO_3 mainly deposits in large pores ($d > 0.7$ nm) and causes a high concentration of HS^- in the water films, where H_2S is predominantly oxidized to elemental sulfur. On the other hand, because of a low concentration of HS^-, a high concentration of O*, and a high surface energy, H_2S is mainly oxidized to sulfuric acid in the small micropores ($d < 0.7$ nm).

5. Conclusions

In this article, the effect of pore structure on the oxidation of H_2S over Na_2CO_3-impregnated activated carbon fibers is discussed. It was found the saturation sulfur capacity of the catalysts depended only on pore structure and was independent of nitrogen functional groups. The products of H_2S oxidation over impregnated ACFs were mainly elemental sulfur and small amounts of sulfuric acid. In small micropores ($d < 0.7$ nm), more sulfuric acid was formed because of the high surface energy and space limitations. In large pores ($d > 0.7$ nm), where most of the Na_2CO_3 deposited, H_2S was predominantly oxidized to elemental sulfur. Because elemental sulfur is the dominant product and mostly deposits in the large pores, the saturation sulfur capacity is mainly determined by the volume of large pores. Therefore, for choosing an effective desulfurization agent, materials with large volumes of pores larger than 0.7 nm and low contents of small micropores seem to be promising.

Acknowledgment

This work was partly supported by the National Science Foundation of China (Nos. 50730003 and 50672025), the National Project of Scientific and Technical Supporting Programs Funded by Ministry of Science & Technology of China (No. 2007BAE55B00), and the National High Technology Research and Development Program of China (No. 2007AA05Z311).

Literature Cited

(1) Ghosh, T. K.; Toleffson, E. L. A Continuous Process for Recovery of Sulfur from Natural Gas Containing Low Concentrations of Hydrogen Sulfide. *Can. J. Chem. Eng.* **1986**, *64*, 960.

(2) Seredych, M.; Bandosz, T. J. Desulfurization of Digester Gas on Catalytic Carbonaceous Adsorbents: Complexity of Interactions between the Surface and Components of the Gaseous Mixture. *Ind. Eng. Chem. Res.* **2006**, *45*, 3658.

(3) Primavera, A.; Trovarelli, A.; Andreussi, P.; Dolcetti, G. The Effect of Water in the Low-Temperature Catalytic Oxidation of Hydrogen Sulfide to Sulfur over Activated Carbon. *Appl. Catal. A* **1998**, *173*, 185.

(4) Bandosz, T. J.; Lee, Q. Evaluation of Surface Properties of Exhausted Carbon Used as H_2S Adsorption in Sewage Treatment Plants. *Carbon* **1998**, *36*, 39.

(5) Turk, A.; Mamood, K.; Mozaffari, J. Activated Carbon for Air Purification in New York City's Sewage Treatment Plants. *Water Sci. Technol.* **1993**, *27*, 121.

(6) Bandosz, T. J.; Block, A. K. Removal of Hydrogen Sulfide on Composite Sewage Sludge−Industrial Sludge-Based Adsorbents. *Ind. Eng. Chem. Res.* **2006**, *45*, 3666.

(7) Rebolledo-Libreros, M. E.; Trejo, A. Gas Solubility of H_2S in Aqueous Solutions of *N*-Methyldiethanolamine and Diethanolamine with 2-Amino-2-methyl-1-propanol at 313, 343, and 393 K in the Range 2.5−1036 kPa. *Fluid Phase Equilib.* **2004**, *224*, 83.

(8) Sidi-Boumedine, R.; Horstmann, S.; Fischer, K.; Provost, E.; Furst, W.; Gmehling, J. Experimental Determination of Hydrogen Sulfide Solubility Data in Aqueous Alkanolamine Solutions. *Fluid Phase Equilib.* **2004**, *218*, 149.

(9) Wieckowska, J. Catalytic and Adsorptive Desulphurization of Gases. *Catal. Today* **2004**, *24*, 405.

(10) Pieplu, A.; Saur, O.; Lavalley, J. C.; Legendre, O.; Nedez, C. Claus Catalysis and H_2S Selective Oxidation. *Catal. Rev.−Sci. Eng.* **1998**, *40*, 409.

(11) Duan, H.; Yan, R.; Koe, L. C.; Wang, X. Combined Effect of Adsorption and Biodegradation of Biological Activated Carbon on H_2S Biotrickling Filtration. *Chemosphere* **2007**, *66*, 1684.

(12) Xiao, Y.; Wang, S.; Wu, D.; Yuan, Q. Catalytic Oxidation of Hydrogen Sulfide over Unmodified and Impregnated Activated Carbon. *Sep. Purif. Technol.* **2008**, *59*, 326.

(13) Mykola, S.; Bandosz, T. J. Role of Microporosity and Nitrogen Functionality on the Surface of Activated Carbon in the Process of Desulfurization of Digester Gas. *J. Phys. Chem. C* **2008**, *112*, 4704.

(14) Adib, F.; Bagreev, A.; Bandosz, T. J. Analysis of the Relationship between H_2S Removal Capacity and Surface Properties of Unimpregnated Activated Carbons. *Environ. Sci. Technol.* **2000**, *34*, 686.

(15) Meljac, L.; Perier, L. C.; Thomas, G. Creation of Active by Impregnation of Carbon Fiber: Application to the Fixation of Hydrogen Sulfide. *J. Colloid Interface Sci.* **2004**, *274*, 133.

(16) Bandosz, T. J.; Bagreev, A.; Foad, A.; Amos, T. Unmodified versus Caustics-Impregnated Carbons for Control of Hydrogen Sulfide Emissions from Sewage Treatment Plants. *Environ. Sci. Technol.* **2000**, *34*, 1069.

(17) Yan, R.; Liang, D. T.; Tsen, L.; Tay, J. H. Kinetics and Mechanisms of H_2S Adsorption by Alkaline Activated Carbon. *Environ. Sci. Technol.* **2002**, *36*, 4460.

(18) Chiang, H. L.; Tsai, J. H.; Tsai, C. L.; Hsu, Y. C. Adsorption Characteristics of Alkaline Activated Carbon Exemplified by Water Vapor, H_2S, and CH_3SH Gas. *Sep. Sci. Technol.* **2000**, *35*, 903.

(19) Xiao, Y.; Wang, S.; Wu, D.; Yuan, Q. Experimental and Simulation Study of Hydrogen Sulfide Adsorption on Impregnated Activated Carbon under Anaerobic Conditions. *J. Hazard. Mater.* **2008**, *153*, 1193.

(20) Tan, X.; Li, X.; Wu, D.; Yuan, Q. Removal of H_2S by Catalytic Oxidation with Impregnated Activated Carbon at Ambient Temperature. *Petrochem. Technol.* **1995**, *24*, 716.

(21) Bagreev, A.; Bandosz, T. J. A Role of Sodium Hydroxide in the Process of Hydrogen Sulfide Adsorption/Oxidation on Caustic-Impregnated Activated Carbons. *Ind. Eng. Chem. Res.* **2002**, *41*, 672.

(22) Yan, R.; Chin, T.; Ng, Y. L.; Duan, H.; Liang, D. T.; Tay, J. H. Influence of Surface Properties on the Mechanism of H_2S Removal by Alkaline Activated Carbons. *Environ. Sci. Technol.* **2004**, *38*, 316.

(23) Ros, A.; Lillo-Rodenas, M. A.; Canals-Batlle, C.; Fuente, E.; Montes-Moran, M. A.; Martin, M. J.; Linares-Solano, A. A New Generation of Sludge-Based Adsorbents for H_2S Abatement at Room Temperature. *Environ. Sci. Technol.* **2007**, *41*, 4375.

(24) Steijns, M.; Mars, P. The Role of Sulfur Trapped in Micropores in the Catalytic Partial Oxidation of Hydrogen Sulfide with Oxygen. *J. Catal.* **1974**, *35*, 11.

(25) Liang, X.; Chen, Q.; Liu, X.; Xu, S.; Wang, Z.; Qiao, W.; Ling, L. Novel Globular Active Carbon and Use in Desulfuration Field. Chinese Patent CN 101347718 (A), 2008.

(26) Sing, K. S. W.; Everett, D. H.; Haul, R. A. W.; Moscou, L.; Pierotti, R. A.; Rouquerol, J.; Sierotti, R. A. Reporting Physisorption Data for Gas/Solid Systems with Special Reference to the Determination of Surface Area and Porosity. *Pure Appl. Chem.* **1985**, *57*, 603.

(27) Le Leuch, L. M.; Subrenat, A.; Cloirec, P. L. Hydrogen Sulfide Adsorption and Oxidation onto Activated Carbon Cloths: Applications to Odorous Gaseous Emission Treatments. *Langmuir* **2003**, *19*, 10869.

(28) Nhut, J. M.; Nguyen, P.; Pham-Huu, C.; Keller, N.; Ledoux, M. J. Carbon Nanotubes as Nanosized Reactor for the Selective Oxidation of H_2S into Elemental Sulfur. *Catal. Today* **2004**, *91*−*92*, 91.

(29) Nhut, J.; Pesant, L.; Tessonnier, J. P.; Wine, G.; Guille, J.; Pham-Huu, C.; Ledoux, M. J. Mesoporous Carbon Nanotubes for Use as Support in Catalysis and as Nanosized Reactors for One-Dimensional Inorganic Material Synthesis. *Appl. Catal. A* **2003**, *254*, 345.

(30) Adib, F.; Bagreev, A.; Bandosz, T. J. Effect of Surface Characteristics of Wood-Based Activated Carbons on Adsorption of Hydrogen Sulfide. *J. Colloid Interface Sci.* **1999**, *214*, 407.

(31) Bandosz, T. J. On the Adsorption/Oxidation of Hydrogen Sulfide on Activated Carbon at Ambient Temperatures. *J. Colloid Interface Sci.* **2002**, *246*, 1.

(32) Bagreev, A.; Menendez, J. A.; Dukhno, I.; Tarasenko, Y.; Bandosz, T. J. Bituminous Coal-Based Activated Carbons Modified with Nitrogen as Adsorbents of Hydrogen Sulfide. *Carbon* **2004**, *42*, 469.

(33) Chang, C. H. Preparation and Characterization of Carbon−Sulfur Surface Compounds. *Carbon* **1981**, *19*, 175.

(34) Adib, F.; Bagreev, A.; Bandosz, T. J. Adsorption/Oxidation of Hydrogen Sulfide on Nitrogen-Containing Activated Carbons. *Langmuir* **2000**, *16*, 1980.

(35) Bagreev, A.; Bandosz, T. J. On the Mechanism of Hydrogen Sulfide Removal from Moist Air on Catalytic Carbonaceous Adsorbents. *Ind. Eng. Chem. Res.* **2005**, *44*, 530.

(36) Klein, J.; Henning, K. D. Catalytic Oxidation of Hydrogen Sulphide on Activated Carbons. *Fuel* **1984**, *63*, 1064.

(37) Adib, F.; Bagreev, A.; Bandosz, T. J. Effect of pH and Surface Chemistry on the Mechanism of H_2S Removal by Activated Carbons. *J. Colloid Interface Sci.* **1999**, *216*, 360.

(38) Katoh, H.; Kuniyoshi, I.; Hirai, M.; Shoda, M. Studies of the Oxidation Mechanism of Sulphur-Containing Gases on Wet Activated Carbon Fiber. *Appl. Catal. B* **1995**, *6*, 255.

(39) Bashkova, S.; Baker, F. S.; Wu, X.; Armstrong, T. R.; Schwartz, V. Activated Carbon Catalyst for Selective Oxidation of Hydrogen Sulphide: on the Influence of Pore Structure, Surface Characteristics, and Catalytically-Active Nitrogen. *Carbon* **2007**, *45*, 1354.

(40) Brazhnyk, D. V.; Zaitsev, Y. P.; Bacherikova, I. V.; Zazhigalov, V. A.; Stoch, J.; Kowal, A. Oxidation of H_2S on Activated Carbon KAU and Influence of the Surface State. *Appl. Catal. B* **2007**, *70*, 557.

(41) Steijns, M.; Koopman, P. The Mechanism of the Catalytic Oxidation of Hydrogen Sulfide II. Kinetics and Mechanism of Hydrogen Sulfide Oxidation Catalyzed by Sulfur. *J. Catal.* **1976**, *42*, 87.

(42) Marsh, H.; Rodriguez-Reinoso, F. *Activated Carbon*; Elsevier: Amsterdam, 2006.

Received for review August 2, 2009
Revised manuscript received February 8, 2010
Accepted February 10, 2010

IE901223J